3

Application of Nanometals Fabricated Using Green Synthesis in Cancer Diagnosis and Therapy

Iliana Medina-Ramirez[1], Maribel Gonzalez-Garcia[2], Srinath Palakurthi[3] and Jingbo Liu[4,5]

[1]*Department of Chemistry, Universidad Autonoma de Aguascalientes, Aguascalientes,*
[2]*Department of Chemistry, Texas A&M University-Kingsville, Kingsville, TX,*
[3]*Department of Pharmaceutical Sciences, Texas A&M Health Science Center, Kingssville, TX,*
[4]*Nanotech and Cleantech Group, Texas A&M University-Kingsville, TX,*
[5]*Department of Chemistry, Texas A&M University, College Station, TX,*
[1]*Mexico*
[2,3,4,5]*USA*

1. Introduction

The interest for the development of new materials for biomedical applications has steadly increased over the past ten years, due to the numerous advances made in the field of cancer diagnosis and therapy using nanoparticles (NPs). Nowadays, these NPs, such as noble metal gold (Au) and silver (Ag), are considered as valuable starting materials for the construction of innovative nanodevices and nanosystems that are built based on the rational design and precise integration of the tailored-functional properties of NPs. The two main goals of this investigation are to: (1) conduct multidisciplinary project and emerging research in the biological and physical sciences to develop new diagnostic methods or cancer therapy tools (health aspect); and (2) optimize the fabrication variables of nano-metals using green colloidal chemistry method (nanotechnological aspect). To accomplish the above goals, we have extensively investigated the fabrication of nano-structured metal(s) using green colloidal (sol-gel) approaches to formulate particles of specific size with defined homogeneity at molecular level; characterized the fabricated nanostructured materials using state-of-the-art instrumentation; and evaluated their *in vitro* cytotoxicity using model cell lines (such as ovarian adenocarcinoma and normal ovarian cell line), and related hemocompatibility of Au and Ag NPs with human red blood cells. The scope of this article will focus on introductory nanoscience, green synthesis strategies, and structural analysis techniques, followed by specific examples related to diagnostics and cancer therapy.

1.1 Source and properties of engineered nanomaterials

1.1.1 General view of nanotechnology

The development of engineered nanomaterials (ENMs) is considered as one of the major achievements of the twentieth century. [1] The novel and outstanding physicochemical properties (which are distinctively different from that of bulk materials) of these ENMs have led to their use in numerous current and emerging technologies. [2] Nowadays, it is practically impossible to find any field of knowledge that is not in some way or another related with nanomaterials; for instance, development of diagnostic sensors for biomedical and environmental applications. [3] In biology and medicine, sensors are being used as DNA/protein markers for disease identification, or as novel drug carriers with little or no immunogenicity and high cell specificity. [4] In materials science, ENMs are currently being used for the development of solar cells, light-emitting diodes (LEDs), information recording systems and non-linear optical devices. [5] Although ENMs represent numerous advantages in their applications, a number of significant challenges still remain in order to ensure the implementation of synthetic pathways that allow for controlled production of all nanomaterials with desired size, uniform size distribution, morphology, crystallinity, chemical composition, and microstructure, which altogether result in desired physical properties. [6] Another important consideration for the practical application of these materials is the high cost associated to their large scale production, coupled with the tremendous difficulties in separation, recovery, and recycling in industrial applications. [7]

1.1.2 Properties of nanomaterials

Nanostructured materials display three major unique properties not observed in their bulk counterparts. [8] They possess: 1) "ultra high surface effect" allowing for dramatic increase in the number of atoms in the surface. [9] When the nanosize is reduced to about 10 nm, the surface atoms account for 20 % of the total atoms composed of the perfect particles. If the particle size is further decreased to 1 nm, the surface atoms account up to 99 % of the total number of atoms. [10] Due to the lack of adjacent atoms, there exist large amount of dangling bonds, which are not saturated. Those atoms will bind with others to be stabilized. This process results in lower than the maximum coordination number and increased surface energy, collectively resulting in high chemical reactivities of the generated nanomaterials; 2) "ultrahigh volume effect" allowing for light weight of small particles. [11] Due to the reduction in the diameter of the nanomaterials, the energy gap was increased. Herein, the electrons are mobile relative to the bulk. This causes unique physical, chemical, electronic and biological properties of nanomaterials compared with macroscopic systems; and 3) "quantum size effect" allowing for nanosize decrease and quasi-discrete energy of electron orbital around the Femi energy level. [12] This will increase the band gap between highest occupied molecular orbital (HOMO) and lowest unoccupied molecular orbital (LUMO), shown in *Fig. 1.* Therefore, the electromagnetic quantum properties of solids are altered. When the nanometer size range is reached, the quantum size effect will become pronounced, resulting in abnormal optical, acoustic, electronic, magnetic, thermal and dynamic properties. The above energy gap (δ) of conduction and valence band of metals was determined by Kubo using an electronic model, $\delta=4E_f/3N$, where the E_f stands for Fermi enegy, N the total electrons in the particles. [13]

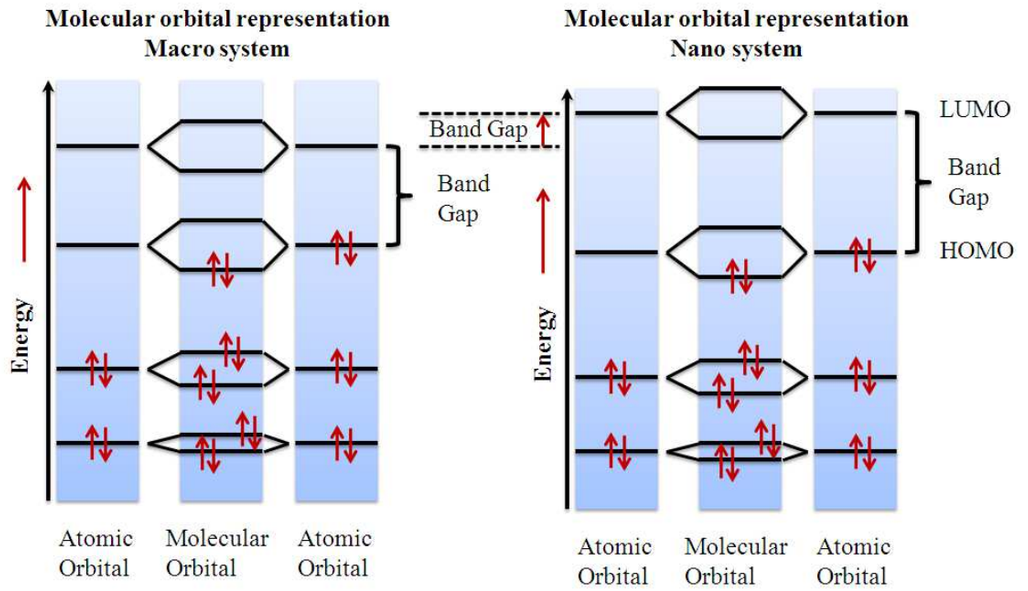

Fig. 1. The band gap between HOMO and LUMO (note: the band gap of nanosystem was increased compared with macrosystem).

1.1.3 Synthesis of nanomaterials

The development of cost-effective environmental friendly methods for large-scale synthesis of benign, highly efficient nanomaterials represents a critical challenge to their practical applications in biomedical research. [14] Some nanoporous materials with regular shapes such as porous nanowires, nanotubes, spheres, and nanoparticles have been successfully prepared by chemical or physical methods which can be carried out in a variety of ways, such as in the gas phase, or in solution, or supported on a substrate, or in a matrix. [15] Although a comprehensive comparison of these approaches does not exist, significant differences in the physicochemical properties, and therefore performance of the resulting materials does exist, allowing for some quantative assessment. In general, physical methods (also known as "top-down" techniques, *Fig. 2*) are highly energy demanding, besides, it is difficult to control the size and composition of the fabricated materials. [16] In the top-down method, the bulk is "broken" down to the nanometer length scale by lithographic or laser ablation-condensation techniques. [17] Chemical methods (also known as "Bottom-up" techniques, *Fig. 2*) are the most popular methods of manufacturing nanomaterials. [18] They are characterized by narrow nanoparticles size distribution, relative simplicity of control over synthesis, and reliable stabilization of nanoparticles in the systems; besides, kinetically controlled mixing of elements using low temperature approaches might yield nanocrystalline phases that are not otherwise accessible. [19] These methods are based on various reduction procedures involving surfactants or templating molecules, as well as thermal decomposition of metal or metal-organic precursors. [20] The sol-gel process has proved to be very effective in the preparation of diverse metal oxide nanomaterials, such as films, particles or monoliths. [21] The sol-gel process consists of the hydrolysis of metal alkoxides and subsequent polycondensation to form the metal oxide gel. [22] One means of achieving shape control is by using a static template to enhance the growth rate of one crystallographic phase over another. [23] The organic surfactants may be undesired for many

applications, and a relatively high temperature is needed to decompose the material. [24] Unfortunately, such thermal treatment generally induces dramatic growth of nanoparticles such that ultrafine nanoparticles free of templating and stabilizing agents could not be obtained [25] Lately, novel and simple methods to prepare metal oxides with controllable morphologies by simply varying the hydrolytic conditions have been reported. [26]

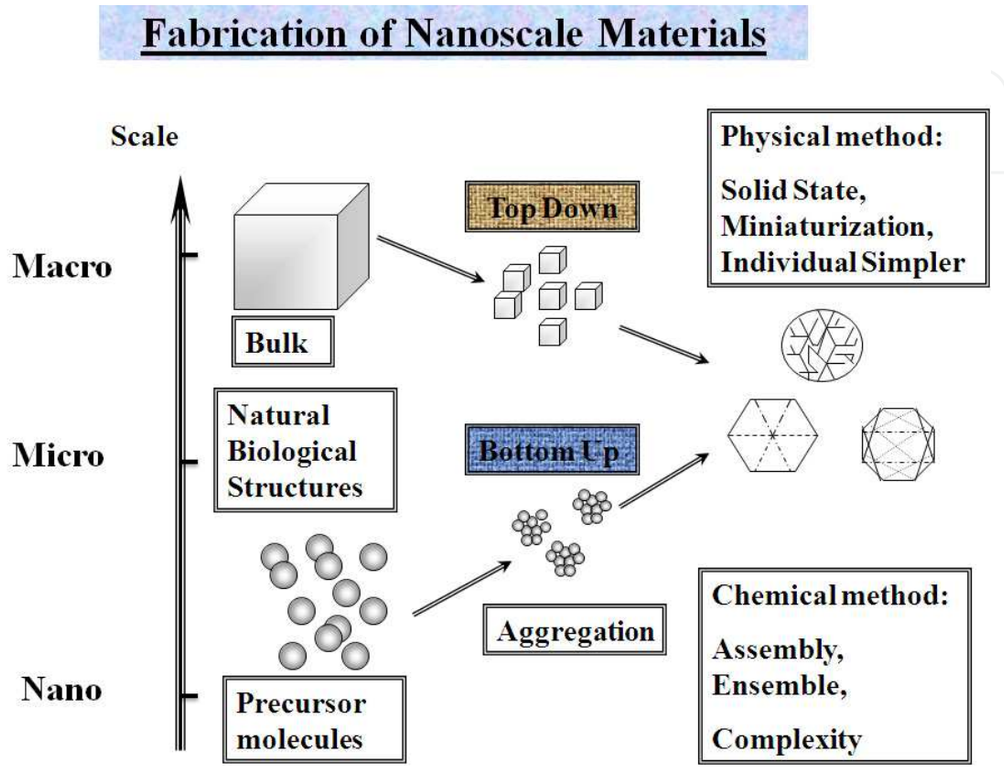

Fig. 2. Schematic of Bottom-up and Top-down Fabrication.

1.2 Toxicological effects of engineered nanomaterials

Metal based nanoparticles (NPs) have been widely used in various applications including biological diagnostics, cell labeling, targeted drug delivery, cancer therapy, and biological sensors and also as antiviral, antibacterial and antifungal agents. [27] An understanding of the potential toxicity induced by these NPs to human health and environment is of prime importance in development of these NPs for biomedical applications. The metal NPs can enter the body via routes such as the gastrointestinal tract, lungs, intravenous injection and exposure in skin. When NPs come to contact with biological membranes, they pose a threat by affecting physiology of the body. For example, silver (Ag), copper (Cu) and aluminum (Al) NPs may induce oxidative stress and generate free radicals that could disrupt the endothelial cell membrane. It was reported recently that in utero exposure to NPs present in exhaust of diesel affects testicular function of the male fetus by inhibiting testosterone production. [28] In this section toxicity issues of each metal nanoparticle will be discussed, starting with aluminum followed by gold, silicon, copper, titania and ceria. Al NPs are widely used in military applications such as fuels, propellants, and coatings. Thus, exposure of aluminum to soldiers and other defense personnel is on the rise. Recent

studies by Wagner *et al* showed that Al NPs exhibit higher toxicity in rat alveolar macrophages and also their phagocytic ability is diminished after 24 h of exposure. [29] Al NPs have produced significant increase in lactate dehydrogensae (LDH) leakage and were shown to induce apoptosis after exposing them to mammalian germline stem cells. [30] *In vivo* toxicity experiments of aluminum oxide nanoparticles in imprinting control region (ICR) strained mice indicated that nano-alumina impaired neurobehavioral functions. Furthermore, these defects in neurobehavioral functions were shown to be mediated by mitochondrial impairment, oxidative damage and neural cell loss. [31]

Gold (Au) NPs are recently widely used in cellular imaging and photodynamic therapy. Au NPs exhibited size-dependent toxicity with smaller-sized particles showing more toxicity than larger-sized particles in various cell lines *in vitro*, and *in vivo* similar pattern of size dependent toxicity was observed. [32] The effect of shape of the Au NPs on toxicity was also assessed and it was reported that Au nanorods were more toxic than spherical Au NPs. [33] The effect of surface chemistry of Au NPs was investigated in monkey kidney cells (CV-1) in and cells carrying SV40 genetic material (Cos-1 cells), and *Escherichia coli* (*E. coli*) bacteria. The results indicated that cationic Au NPs were more toxic compared to their anionic counterparts. [34]. Lately, biofuncionalization (Lysine capped) of Au NPs has been explored in an attempt to reduce their toxicity. These lysines capped Au NPs were not toxic to macrophages at concentrations up to 100 μM after 72 h exposure. Moreover, they did not elicit the secretion of pro-inflammatory cytokines tumor necrosis factor-alpha (TNF-α) or interleukin-1 beta (IL-1β). [35]

Silicon microparticles were investigated for their biomedical application; the results have shown that vascular endothelial cells which internalized silicon microparticles maintained their cellular integrity as demonstrated by cellular morphology, viability, and intact mitotic trafficking of vesicles bearing silicon microparticles. [36] Silica (SiO_2) NPs were also investigated for their toxicity as they promise effective biomedical applications. When SiO_2 NPs were treated on normal human mesothelial cells at concentration of 26.7 μg/mL, there was only 3% LDH leakage after 3 hr exposure. When mice were treated with SiO_2-nanoparticle coated magnetic nanoparticles for 4 weeks, the NPs were shown to be taken up by the liver and then redistributed to other organs such as spleen, lungs, heart, and kidney. It was also reported that NPs (<50 nm) bypassed various biological barriers (blood-brain and blood-testis) without inducing any toxicity. [37] The Ag NPs have also shown cellular toxicity; *in vitro* they exhibited size and dose dependent toxicity in neuroendocrine cells, liver cells, lung cells and germline stem cells, and the toxicity was reported to be mediated mainly through oxidative stress. *In vivo,* these NPs of 60 nm size were investigated at various doses (30, 300 and 1000 mg/kg) and these NPs showed a dose dependent liver toxicity. [38] Copper (Cu) nanoparticles are widely investigated for their antimicrobial properties. Cu NPs, though very effective antimicrobials, exhibited severe toxicological effects including heavy injuries in kidney, liver, and spleen of mice after administration. [39,40]

Titanium dioxide (TiO_2) nanoparticles are very widely manufactured nanomaterials for various applications including cosmetics, paints and as additives to surface coatings. TiO_2 NPs have shown to induce inflammatory responses and reactive oxygen species (ROS) in various cell types and tissues. [41] However, Renwick *et al* reported that TiO_2 NPs were not directly toxic to macrophages but significantly reduced the ability of macrophages to phagocytose other particles. [42] Cerium oxide (CeO_2) nanoparticles were recently used in computer chip manufacturing, polishing and as an additive to decrease diesel emissions.

The toxicity studies of CeO_2 nanoparticles involving human lung adenocarcinoma epithelial cell line (A549 lung cells) have shown that CeO_2 NPs did not result in any significant change in LDH leakage or cell morphology, but exhibited a NP induced oxidative stress resulting in altered gene expression. [43]

Hemocompatibility of metal nanoparticles is a very important property for biomedical applications. Metal nanoparticles with good hemocompatibility are often desirable since red blood cells are the primary cells that come in contact with metal nanoparticle when administered intravenously. Various attempts were made to improve the hemocompatibility of metal nanoparticles. It was reported that when Zein, a natural polymer, was incorporated into silver NPs, the hemocompatibility was easily achieved. The results indicated that zein-silver nanocomposites have shown better hemocompatibility when compared with Ag NPs alone. [44,48-49] Ren *et al* have investigated the hemocompatibility of cisplatin loaded Au-Au2S nanoaparticles. The results indicated that bare Au-Au2S NPs have shown hemolysis ratio below 2 % at 100 μg/mL concentration. The cisplatin loaded Au-Au2S nanoparticles have shown hemolysis ratio < 5% at 80 μg/mL, indicating their hemocompatibility and potential use for cancer therapy. [45]

1.3 Nanostructural characterization of engineered nanomaterials

We have been able to synthesize several metallic and semiconducting NPs, which have been evaluated using several state-of-the-art instrumentation techniques. Spectroscopic and microscopic techniques were employed in order to determine the stability, crystalline phase, morphology and size distribution of the synthesized NPs.

1.3.1 Surface energy study of engineered nanomaterials

The electrokinetics (expressed by zetapotential, ζ) of the colloidal suspension was measured using a ZetPALS approach to evaluate particle size and its distribution, from which the stability of engineered nanomaterials can be further determined. [46] Based on the sign of particle's, ζ, the charge can be also determined. [47] The time dependence of the zetapotential on the course of measurement is another technique to understand the formation mechanism of nanoparticles. It was encountered that the large zetapotential of the like (negative) charges enabled to minimize the particles agglomeration due to electrostatic repulsion.

1.3.2 Crystalline phase study of engineered nanomaterials

X-ray powder diffraction (XRD) analysis was used to identify the crystalline phase of the NPs due to its capability to provide rapid, non-destructive analysis of multi-component mixtures, allowing quick and accurate analysis of phase, crystallinity, lattice parameters, expandition tensors and bulk modules, and aperiodical arranged clusters. Based on the peak broadening, the cyrstallite size can also be calculated using Scherrer equation. [50] XRD characterization is widely used in various fields as metallurgy, mineralogy, forensic science, archeology, condensed matter physics, and the biological and pharmaceutical sciences. *Fig. 3* display the working principle and major information obtained from XRD.

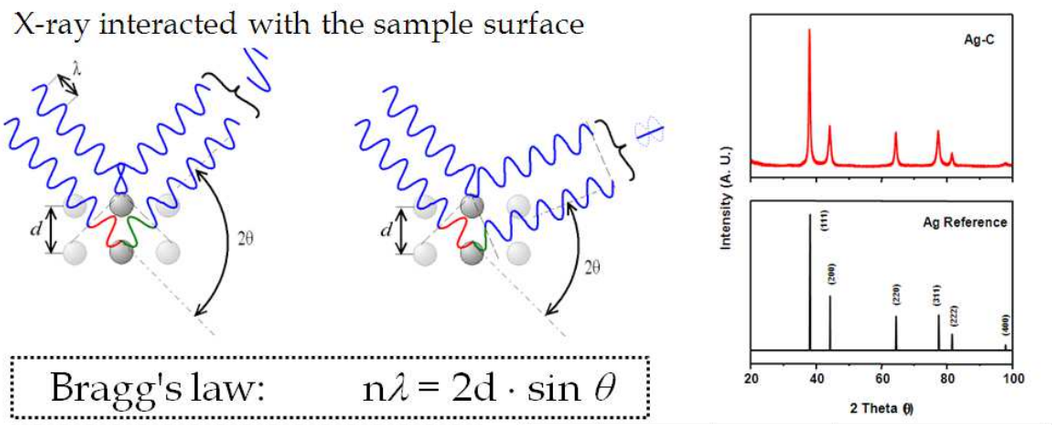

Bragg's law: $n\lambda = 2d \cdot \sin\theta$

Scherer equation:

$$\beta_{hkl} = \frac{K\lambda}{L_{hkl} \cdot \cos\theta}$$

	Crystallite size	Crystallinity	Particle Type
Ag-a	13	~1.2	monocrystalline
Ag-b	27	~1.2	monocrystalline
Ag-c	62	~3.5	Polycrystalline

n is an integer determined by the order given, λ is the wavelength of x-rays (nm), and moving electrons, protons and neutrons, d is the spacing between the planes in the atomic lattice (nm), θ is the angle between the incident ray, and the scattering planes (rad) , L is the crystallite size (nm), β is the full width at half maximum (rad), and K is a constant, that varies with the method of taking the breadth (0.89<K<1).

Fig. 3. XRD characterization of nano-materials.

1.3.3 Fine-structure study of engineered nanomaterials

In this study, the morphology and crystalline structure of the engineered nanomaterials were characterized using scanning and transmission electron microscopy (SEM and TEM). [51] Both techniqes are based on the use of a microscope that uses high energy electrons to form an image. Due to their advantages of higher magnification, larger depth of focus, greater resolution, and ease of sample observation, both facilities have been employed widely to determine the crystalline phase, defects, and texture of materials. [52] High resolution field emission TEM was employed to achieve high spatial resolution, high contrast, and unsurpassed versatility. Particularly, the Tecnai F20 G² TEM used in this study, which includes a Schottky field emission source, provides ultra-high brightness, low energy spread and very small probe sizes. The Tecnai F20 G² used in this study has been designed and preconfigured specifically to meet the strict requirements of nanomaterials. This TEM is also equipped with a robust high-brightness field emission gun, allowing for a wide range of applications, from morphological analysis to defect characterisation. [53]

1.3.4 Elemental composition study of engineered nanomaterials

As complementary techniques, energy dispersive spectroscopy (EDS, equiped with TEM) and X-ray photoelectron spectroscopy were used to accurately determine the elemental composition. [54] The EDS is normally used as a semi-quantitative analysis that allows for determination of the amount and identity of the different elements. The EDS can stimulate

the emission of characteristic X-rays from a specimen, herein, a high energy beam of charged particles (electrons, protons) is then produced and focused into the sample. An atom within the sample contains ground state electrons in discrete energy levels or electron shells bound to the nucleus. [55] The incident beam form EDS may excite an electron in an inner shell, ejecting it from the shell and creating an electron hole. An electron from an outer, higher-energy shell then fills the hole. The difference in energy may be released in the form of an X-ray. The number and energy of the X-rays emitted from a specimen can be measured by an energy dispersive spectrometer. As the energy of the X-rays is characteristic of the difference in energy between the two shells, and of the atomic structure of the element from which they were emitted, this allows the elemental composition of the specimen to be measured. The principle of EDS is also shown in *Fig. 4* (see § 1.3.3 *Fine-structure study of engineered nanomaterials*).

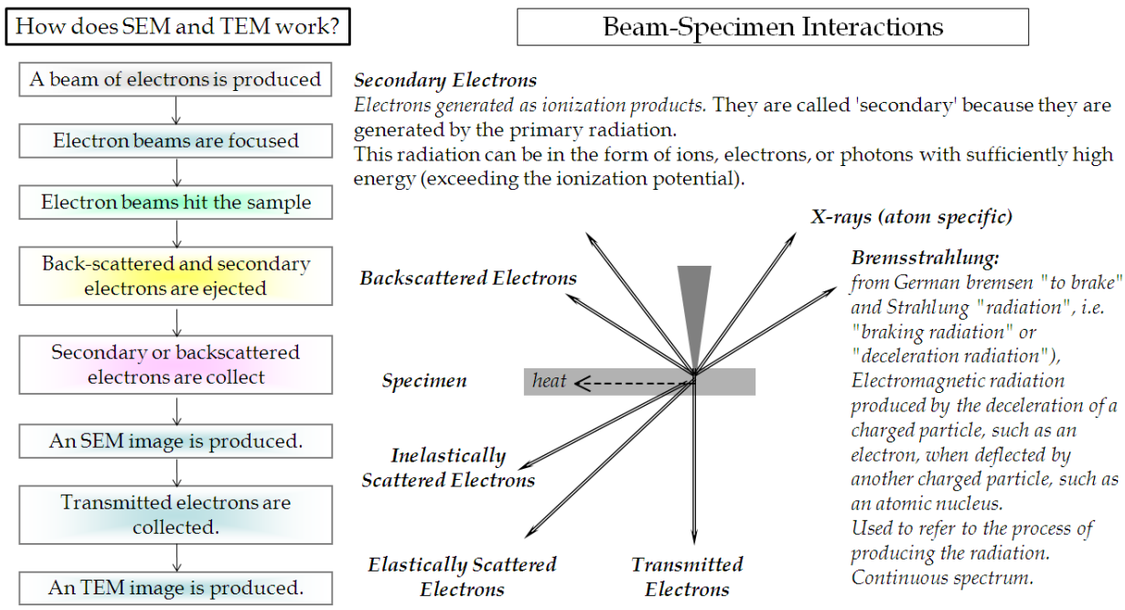

Fig. 4. Schematic demonstrates the working principle of TEM (SEM included).

XPS is a surface chemical analysis technique (*Fig. 5*), which can irradiate a material with a beam of aluminum (Al) or magnesium (Mg) X-rays. [56] Measurement of kinetic energy (KE) and binding energy (BE) can be completed by determining the number of electrons that escape from the top within 1 to 10 nm. Both EDS and XPS require ultra-high vacuum (UHV) conditions to provide uniformity of elemental composition across the top of the surface. [57] Additionally, XPS can also provide uniformity of elemental composition as a function of depth by ion beam ablation and by tilting the sample, empirical formula of pure materials, elements that contaminate a surface, and chemical or electronic state of each element in the surface. An analysis of titanium (Ti) is selected for demonstration. Based on the binding energy, the element can be determined; such as Ti can be identified via measurement of its binding energies of Ti $2p_{3/2}$ and Ti $2p_{1/2}$ electron configurations located at 456.3 electron-volt (eV, ~1.602×10^{-19} C) and 462.2 eV, respectively. In addition, the difference in binding energy can be used for indexing, since the difference in binding energy for the peak splitting of Ti $2p_{3/2}$ and Ti $2p_{1/2}$ was calculated to be 5.9 eV. From this analysis, it can be concluded

that Ti was well-indexed with the standard Ti 2p binding energies and their difference ($2p_{3/2}$ = 454.1 eV, $2p_{1/2}$ = 460.3 eV, Δ= 6.2 eV). [58]

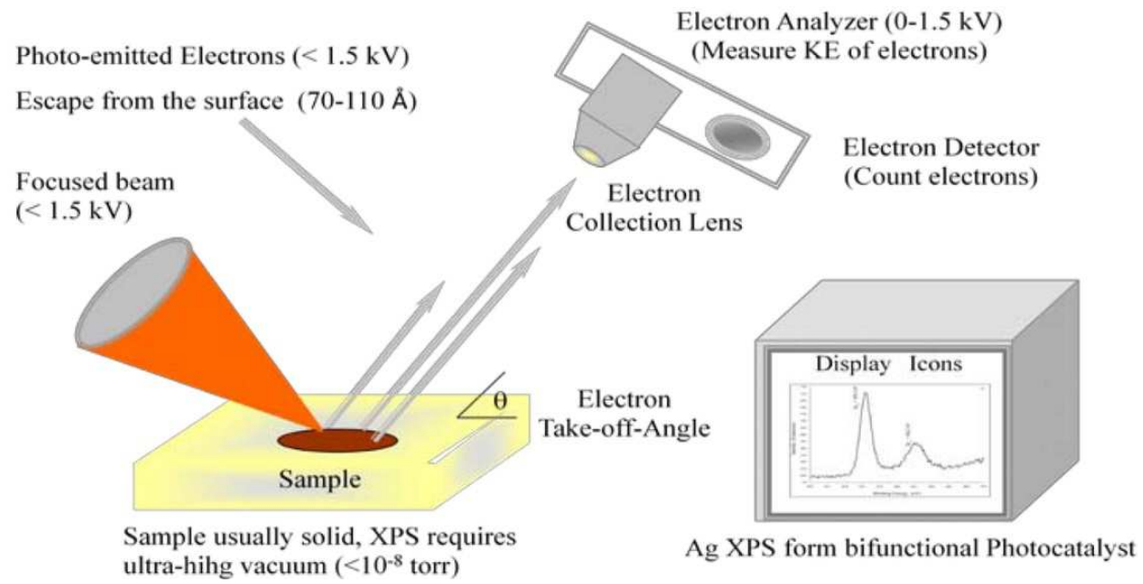

Fig. 5. Demonstration of how XPs works and information obtained.

1.4 Biomedical application of engineered nanomaterials

The most important driving force behind many changes in the field of medical research is the advent of nanotechnology. Progress in nanotechnology is not only aiming at miniaturization but also at systems with increased complexity. This is not just a matter of geometrical structurization but also a matter of specific functionalities that are positioned at discrete locations and in defined distances. Whereas many NMs exhibit localization to diseased tissues via intrinsic targeting, the addition of targeting ligands, such as antibodies, peptides, aptamer, and small molecules, facilitates far more sensitive cancer detection. Nanoparticles with certain specific surface characteristics such as charge and hydrophobicity along with enhanced permeability and retention effect (EPR) have shown higher bioavailability at the target site. EPR is a result of disorganized angiogenesis leading to production of "leaky" blood vessels. EPR effect and lack of effective lymphatic drainage in the tumor tissue have improved the chances of nanoparticle imaging agents with sizes 10-100 nm to be retained in tumor. [59]

Use of nanoparticles in imaging for cancer broadly encompasses two wide areas: (1) detection of certain protein or cancer cells using nanoparticles and, (2) formulation of nano-imaging agents to improve the specificity and to provide high-contrast imaging. Capturing of circulating tumor cells has great potential in cancer diagnosis and therapy. It is very challenging because of the fact that on an average there may be only 1-2 cancer cells per milliliter of blood. Nanotechnology devices based on molecular biomarkers have shown great promise in improving the yield of cancer cell captured. [60] For example, to improve the detection sensitivity and specificity, folate conjugated gold-plated carbon nanotubes were used as contrast agent for photoacoustic imaging. [61]

Many nanoparticle based devices were investigated for their potential applications for imaging in tumor therapy. Most of these were investigated at preclinical stage with few reaching clinical trials. The nanoparticles investigated are either monofunctional or multifunctional. Quantum dots (QDs), which are colloidal fluorescent semiconductor nanocrystals, have sizes ranging from 2-10 nm were investigated in visualization of colon cancer using fiber optics. [62] Iron oxide Nanoparticles conjugated with herceptin as targeting ligand were investigated for detection of small tumors of breast cancer using magnetic resonance imaging (MRI). [63] Dendrimers which are highly branched synthetic polymers were conjugated with prostate specific antigen and were used for imaging in prostate cancer. [64]

Multifunctional nanoparticles are the nanoparticles which combine various functionalities to improve specificity to cancer cells at a single component. Silica based nanoparticles are considered to be promising candidates for development of multifunctional nanoparticles because of their ability to host various materials such as fluorescent dyes, metal ions and drugs. [65] Supramagnetic iron oxide nanoparticles coated with silica were conjugated with fluorescein isothiocyanate to label human bone marrow mesenchymal stem cells. [66]

The most recent nanoparticles also termed as third-generation nanoparticles involve a disease-inspired approach of the "nanocell" which are nanoparticle constructs that comprise a polymeric nanoparticle core enclosed in a lipid-based nanoparticle. For example, an anti-angiogenic agent (combretastatin) will be trapped in the lipid envelope and polymeric nanoparticle core will be loaded with a conventional chemotherapeutic agent like doxorubicin. This nanocell when accumulated in tumor by EPR effect will effectively disrupt the tumor vascular growth by releasing the anti-angiogenic agent followed by release of cytotoxic agent for effective tumor inhibition. [67]

1.4.1 Mechanistic study of cancer theragnostics

Relevant biomedical applications of new nanomaterials are cancer diagnosis and treatment. Nanotechnology offers opportunities to enhance our understanding of the mechanisms of cancer, such as by detecting the generation and distribution of cancer cells in tissues, which can lead to improved diagnosis of this dreadful disease. Furthermore, by harnessing and targeting the toxic properties of nanoparticles, therapeutic agents that are more effective for treating cancer will be developed through molecular targeting.

Cancer encompassess a set of complex and diverse diseases that arise generally when normal cells are transformed into tumorogenic cells, which grow in an uncontrolled fashion to the detriment of the surrounding tissues and eventually the organism. Several factors can play a role in the generation and aggressiveness of the tumor cells, such as accelerated growth, lack of need for growth factors or absence of response to growth inhibitors, unresponsiveness to factors that trigger cell death by apoptosis, enhanced migration properties and ability to invade blood circulation, evasion of the immune response, etc. [68] Mechanistically, the transformed phenotype is derived from the progressive accumulation of genetic mutations, including base changes, nucleotide additions and deletions, insertions, duplications, and chromosomal translocations. [69] Many types of genes have been associated with the development of cancer, such as oncogenes, tumor suppressor genes, apoptosis regulatory genes, cell cycle genes, invasiveness and metastasis related genes, etc. [68-73]

One major difficulty in the treatment of cancer is that the tumor cannot often be detected early enough in patients. Early stage tumors usually have favorable prognosis, while many larger, more developed tumors are frequently refractory to current anti-cancer therapies. Another major problem of many current therapies is the lack of adequate selectivity for cancer cells. This inability to adequately distinguish between cancer and normal, healthy cells, leads to toxic effects on the normal cell population and, therefore, detrimental side effects on the cancer patient. The use of NPs in anti-cancer therapies may improve tumor therapies in these two fronts.

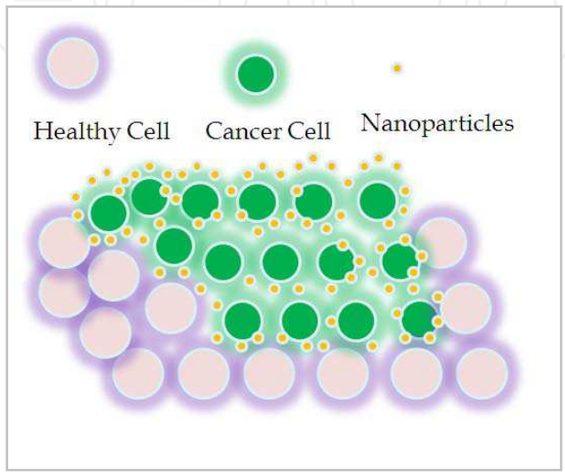

Fig. 6. Detection of cancer cells using NPs.

Different types of metal nanoparticles can be modified to expose molecules that confer them selective binding to specific molecules on the surface of cancer cells, providing probes for the detection and monitoring of cancer cells in tissues (*Fig. 6*). Au NPs in particular have long been utilized in the specific detection of molecules at the surface or inside cells. [74] Other nanomaterials with different chemical reactivity characteristics, including reactivity towards specific functional groups or surface oxidation properties, could provide certain advantages for performing modifications that confer targeting properties to the NPs. The changes in surface plasmon resonance (SPR) properties of Au and Ag NPs caused by interactions with molecules in the surrounding environment can be applied in sensing biomolecules on the surface of tumor cells.

Detectors based on such sensors can be very useful for the early detection of cancer cells (*Fig. 7*). The use of Au NPs is also being explored for the early detection of tumors by other techniques such as X-ray scatter imaging . [75] In this research, hepatocellular carcinoma cells containing Au NPs coated with two layers of charged polymers showed enhanced X-ray scattering over cells containing no gold. Hepatocellular carcinoma is the most common cancer that affects the liver and has an estimated 5-year survival rate of only 10%, since current detection methods can only spot the tumors when they have grown to about 5 centimeters in diameter. The imaging technique utilized by this research group (spatial harmonic imaging, SHI) in combination with targeting of the Au NPs to hepatocellular carcinoma cells via attachment to a specific antibody (FB50) has the potential to detect tumors of only a few millimeters in diameter, which would very significantly improve the prognosis of this cancer type.

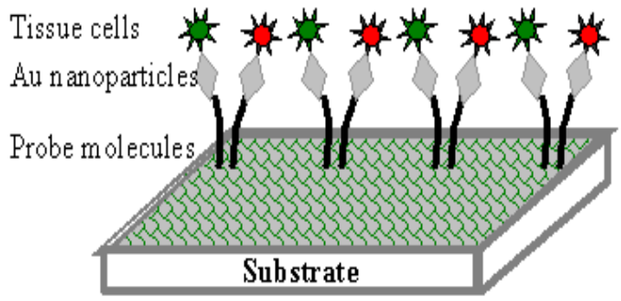

Fig. 7. Schematic design for cancer imaging via optically/electrochemically active gold-NPs.

As indicated, the use of nanomaterials is being investigated not only for the early detection of tumors, but also for the specific destruction of cancerous cells. Ag NPs disrupt the function of proteins and other macromolecules on the surface of bacterial and eukaryotic cells, which can lead to permanent damage and death of the cells. [76-77] Other metallic NPs have different toxicity effects on cells. TiO_2 NPs for example do generate reactive oxygen species (ROS) upon absorption of ultraviolet (UV) light. Additionally, specific modifications of the metallic NPs can attach other toxic molecules to the nanomaterial. Combining the toxicity effects of novel nanomaterials with specific targeting to tumor cells can lead to the development of highly specialized therapeutic NPs that can be introduced into the body of cancer patients, where they could detect and destroy cancer cells at early stages, preventing the growth of tumors.

Molecular targeting of NPs was utilized in the generation of TiO_2 NPs coupled with an antibody, which targeted the nanomaterial to glioblastoma multiforme cancer cells (glioblastoma multiforme is a type of brain cancer). [78] The antibody used recognizes the interleukin-13 receptor α2 protein chain (IL13Rα2), which has been shown to be almost exclusively overexpressed on the plasma membrane of certain brain tumors, including glioblastoma multiforme. [78-80] The nanomaterial accumulated inside tumor cells and upon exposure to UV light, the NPs led to the formation of ROS and killed the cancerous cells, while they did not show citotoxicity toward normal brain cells.

An example of NPs application for drug delivery is the formation of "Trojan horse" like hybrid NPs. Glycan NPs were synthesized using cyclodextrins as stabilizing agent (polymeric backbone). These glycan NPs were used as envelope for the encapsulation of camptothecin. The formulation of the NPs allowed its internalization on tumor cells; inside the tumor cells, the coating is desintegrated, releasing the toxic molecule that destoys specifically the tumor cell without harming healthy cells. [81] This glycan NPs containing camptothecin, designated as IT-101, have been shown to eliminate or significantly reduce tumors in several mice models of human cancer, and are currently under investigation in clinical trials for the treatment of cancer patients. Delivery of these glycan NPs to tumors is based on the fact that newly formed tumor blood vessels are leaky and let particles as large as 400 to 700 nm into the cancerous mass.

2. Experimental approach

Here, we describe design, synthesis and characterization of nanoscaled metals and their nanostructures. All chemicals used are of analytical grade and were obtained from various

vendors. Silver nitrate ($AgNO_3$) and gold (III) chloride trihydrate were purchased from Sigma–Aldrich (St Louis, MO), L-ascorbic acid and other reducing agens from Fisher (Thermo scientific, Pittsburgh, PA), Arabic gum from M.P. Biomedicals, Morgan Irvine, CA), and used without modification. The experiments are carried out for the construction of NPs derived from a bottom-up colloidal method. Non-toxic chemicals and two strong reducants are used in various formulations of NPs, allowing for mitigation of pollution. The structural characterization is by electron microscopy and X-ray diffraction. We also investigated the toxicity of some of the synthesized NPs. Importantly, as previously indicated in the introduction, this approach can also be applied to the toxicity and cancer diagnosis, along the "theragnostics mechanism" described in the following sections.

2.1 Fabrication of nanometals

The experimental workflow to engineer nanoparticles is shown in *Fig. 2* (see §1.1.3 *Synthesis of nanomaterials*). Briefly, the nanometal was created by dissolving different concentrations of silver nitrate ($AgNO_3$) and/or gold (III) chloride trihydrate ($HAuCl_4 \cdot 3H_2O$) in distilled water. Concentration was controlled at 0.005-1.0 M according to application. This aqueous solution was mixed continuously with a magnetic stirrer/mechanical agitation for 30 min. *Arabica* gum (AG, as a surfactant) was added (2 % by mass) to the above solution to improve the dispersion of NPs and to control the particle size. Reducing agents (four selected ones) were then incrementally added into the solution. The molar ratio of metallic cations to reducing agent was controlled at 1:2 to 1:8 and to produce 16 formulations. The colloids were directly used for zetapotential, cytotoxicity and hemocompatibility analyses. The precursor sols were heated between 60 and 80 °C for 2 hrs and filtered and rinsed with ethanol/deionized (DI) water to produce powders used for XRD and and TEM analysis.

2.2 Structural characterization

In tandem to §1.3 (*Nanostructural Characterization of Engineered Nanomaterials*), this section briefly discusses the technical variables or the characterization methods. A ZetaPALS™ (Brookhaven Instruments Corporation, NY) was used to measure the particle size distribution and zeta-potential to evaluate the stability of NPs. The ZetaPALS operating conditions are as follows: An electric field (2 V•cm) was applied to obtain good results. This electric field was used and an alternating current (AC) waveform with the frequency control of 2-20 Hz was applied; measurement duration was kept at 30 to 60 s; laser input was 5 V and laser output power was 35 mW; and an automatic selection of field strength was used. The Ultima III X-ray powder Diffraction (XRD) was employed to determine the crystalline phase and average crystallite size of the NPs. The XRD patterns were collected using a Rigaku multiflex diffractometer, equipped with a copper (Cu) target. The scanning range varied between 30 and 80 degrees at a scanning rate of 2 °/min. The phase structure was then identified through the Jade 7.0 database. A Tecnai F20-G^2 TEM (FEI Company, Tecnai F20-G^2 Hillsboro, OR), equipped with ED and EDS techniques were also employed to obtain nanostructural information, crystalline phase and elemental composition of nanometals. In the EDS analysis, the peak intensities were converted to percent weight and then to final molar ratio via the DAX ZAF Quantification tool. The spectra were acquired to determine elemental composition. The HRTEM images were taken at a direct magnification of 600 thousand magnitudes with the point resolution of 0.2 nm. An Axis ULTRA XPS (Kratos

Analytical Inc, NY) was employed to identify the elemental composition of the products. The operating specifications were: high vacuum was controlled under 10^{-8} Torr; anode mode was aluminum (Al, K_α) monochromatic energy source with the power of 10 mA by 12 kV; the lens was used in hybrid mode; resolution of the individual element analysis was of pass energy of 40 eV and 160 eV for survey. [88]

2.3 Evaluation of *in vitro* cytotoxic activity

The cytotoxicity of Au and Ag NPs was performed in two cell lines: ovarian adenocarcinoma cell line (NCI/ADR-RES), and normal ovarian cell line (NCI/CHO). A total of 2×10^4 cells in 200 μL of medium per well were placed in a 96-well plate. After incubation overnight, the medium was replaced with media containing nanometals at different concentrations (0.1, 0.5, 1, 10, and 100 μM) in separate wells. After 24 hrs of incubation, the medium was removed and the cells were washed with ice-cold phosphate-buffered saline (PBS) three times to remove NPs. A volume of 50 μL of 3-[4, 5-dimethylthiazol-2-yl]-2,5,-diphenyl tetrazolium bromide (MTT) at a concentration of 5 mg/mL was then added to each well. Following incubation for 4 hrs, formazan crystals formed were dissolved in 150 μL of dimethylsulfoxide and absorbance was measured at 530 nm using a NOVOstar plate reader (BMG lab technologies, Cary, NC, USA). The percentage viability was calculated by comparing absorbance of treated cells versus untreated control cells which were assigned 100 % viability.

2.4 Evaluation of hemocompatibility

To evaluate hemocompatibility, human red blood cells (HBCs), which composed of reduced leukocytes with adenine-saline were used. HBCs were obtained from coastal bend blood center, Corpus Christi, Texas as a kind gift from. The HBCs were separated from plasma by centrifugation at 4,000 rpm for 5 min at 4 °C. HBCs were washed three times with physiological saline solution and re-suspended in saline to obtain HBCs suspension at 2% (v/v) hematocrit. The so-prepared HBC-suspension was used within 24 hrs upon preparation.

3. Results and discussion

The optimal fabrication variables of NPs will be discussed first (described in § 3.1), followed by electrokinetic properties analysis and crystalline phase strucure of NPs (described in § 3.2-3.3). The *in-vitro* toxicicity and hemocompatibility will be discussed next (described in § 3.5) and conclusion on bioapplication of nanomaterials to close the chapter (§ 4.0).

3.1 Fabrication optimization of engineered nanomaterials

The generation process of nanoparticles through facile chemical approach is as follows: (1) A complex between a metal ion and a ligand, that is the functional group of a protecting polymer, is formed in an aqueous solution; (2) The metal ion is reduced to a metal atom with a reducing agent; and (3) The metal atoms aggregate and grow into nanoparticles. The effect of the nature and concentration of the reducing agent was evaluated. As "green" reducing agents, ascorbic acid and sodium citrate were employed. As strong reducing agents, sodium borohydride ($NaBH_4$) and dimethylaminoborane (DMAB) were also tested

as the control samples. The concentration of the reducing agent was varied from 1:1, 1:2, 1:4 and to 1:8 molar ratios with respect to metallic ion. Table 1 tabulated the 44 formulations of the nanopartciles via bottom-up "green" colloidal chemistry method. In this study, the reduction of noble metal cation occurs spontaneously. The reactions are shown as follows:

$$Ag+ (aq) + e^- \rightarrow Ag^\circ (s) \qquad E^\circ = +0.80V \quad (1)$$

$$AuCl_4^- (aq) + 3\, e^- \rightarrow Au^\circ (s) + H^+ (aq) + 4\, Cl^- (aq) \qquad E^\circ = +0.99V \quad (2)$$

$$C_6H_8O_6 (aq) + 2\, e^- \rightarrow C_6H_6O_6 (aq) + 2H^+ (aq) \qquad E^\circ = +0.06V \quad (3)$$

According to these three half reaction standard reduction potentials, the overall reaction is determined to have a potential of 0.74 and 0.93 V, respectively. This indicates that the redox reaction between Ag^+ and $C_6H_8O_6$, and $HAuCl_4$ and $C_6H_8O_6$ occurs spontaneously since they are favored, thermodynamically. The released proton H^+ (from both half reactions, the redox process) was responsible for acidity and resulting decrease in pH.

In this research, the dispersing agent, Arabic gum (AG), was used as a size directing agent in the synthesis of the nanometals and to prevent the agglomeration of the fine particles (< 10 nm). Because the complex between surfactant and metal ions can be formed, the growth of the central particle is prevented and terminates at a size in the nanoscale regime (1-100 nm). In short, AG regulates stability of nanoparticles. The synthesis of noble metal nanocomposite via reduction of metal ions in aqueous solutions of AG is based on the formation of a stable metal particle-macromolecular complex.

Cross Product of conc. and molar ratio		Molar ratio of M^{n+} : reducing agent			
		1:1	1:2	1:4	1:8
Concentration of reducing agents and Ag^+ or Au^{3+} (mol/L)	0.005	10 mL * 10 mL**	10 mL 20 mL	10 mL 40 mL	10 mL 80 mL
	0.01	10 mL 10 mL	10 mL 20 mL	10 mL 40 mL	10 mL 80 mL
	0.02	10 mL 10 mL	10 mL 20 mL	10 mL 40 mL	10 mL 80 mL
	0.03	10 mL 10 mL	10 mL 20 mL	10 mL 40 mL	10 mL 80 mL
	. . .	. . .	. . .	. .	. .
	0.5	10 mL 10 mL	10 mL 20 mL	10 mL 40 mL	10 mL 80 mL
	1.0	10 mL 10 mL	10 mL 20 mL	10 mL 40 mL	10 mL 80 mL

Note: * represent the volume of metallic cation solution and ** the volume of reducants.

Table 1. Potential set of values of volume of M^{n+},and reducing agents at designed molar ratio when temperature is maintained at 60 °C and agitation at 1000 rpm.

3.2 Nanocharacterization and bio-application of engineered nanomaterials

The surface energies of nanomaterials are described first in §3.2.1. The crystalline structural, morphological and elemental composition characterization are described next from §3.2.2 to -3.2.4. Lastly, the cytotoxic activity and hemocompatibility of nanometals is described in §3.3 and 3.4, respectively.

3.2.1 Electrokinetic behavior of metallic colloidal suspension

The measured zetapotentials (ζ, with ZetaPALS™) of nanosized metal colloidal suspension were averaged at -44.00 mV. The negative sign indicates large repulsive forces between nanoparticles of either silver or gold preventing flocculation and aggregation of particles and the numerical value indicates samples had colloidal stability (*Fig. 8*). ζ results indicate that the colloid of Ag and Au are stable and agglomeration is successfully prevented using GA as the surfactant. The electrokinetic study also confirms that nano-dispersion of Au with size of 10-15 nm (correspondingly, the particle size of NP powders were found by TEM, see *Fig. 10 a & b*) has been achieved. Fluctuations in the measured value of ζ during the experiment were not observed; therefore the measurements were time independent in the present study, which confirms the stability of nanometal colloid.

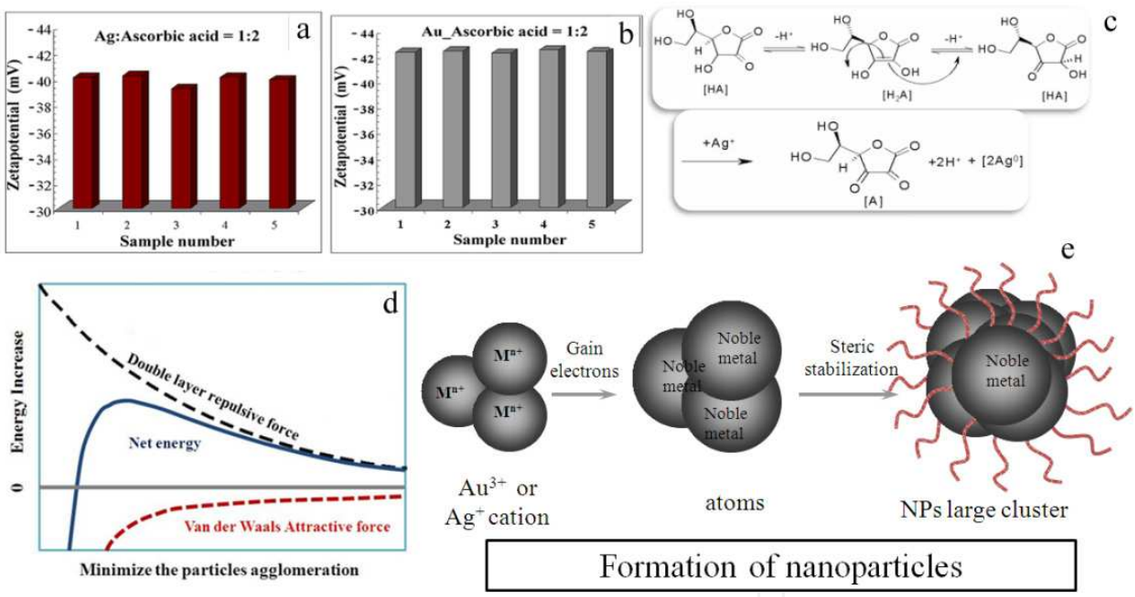

Fig. 8. Relationship between particle size and zetapotential, a: the zetapotential measurement to determine the surface energy of silver nanoparticles, b: the zetapotential measurement to determine the surface energy of gold nanoparticles, c: redox reaction to obtain nanometal particles, d: repulsive and attractive forces in colloidal suspension, and e: schematic of repulsive or attractive forces on nanoparticles, the magnitude which defines aggregation, or separation.

The main goal during the synthesis phase was to control the particle size and its morphology followed by nanocharacterization of the nanoparticles. These particles were synthesized using a bottom-up colloidal chemistry approach. Ag and Au-NP size was

controlled through incorporation of GA as the dispersing agent, which also aids wetting of the metal salt. The large negative zetapotential would promote repulsion between the nanoparticles, which in turn would minimize particles agglomeration, which is schematically summarised in *Fig. 8e* (see above figure). The contribution of this green synthesis lies in the following: 1) Finding the best fabrication parameters to achieve complete de-aggregation of the nanoscaled catalyst; 2) Identifying non-toxic dispersing agents to prevent aggregation of the nanocatalyst; and 3) Identifying the suitable reducing agent that ensures complete reduction of metal ions and improves the mono-dispersion of nanocatalyst.

3.2.2 Crystalline phase analyses of engineered nanomaterials

XRD results can provide figure-print characterization of the crystalline phase and the lattice constants. *Fig. 9a* indicates that Ag-NPs display highly crystalline face centered cubic (fcc) space group. The Ag NPs derived from green colloidal chemistry is well indexed with PDF 01-089-3722 (lattice constants, a = 4.0855 Å and α = 90°). In addition, the crystallite size was calculated to be averaged at 30.2 nm. According to the full width at half maximum, the crystallite size was calculated using Scherrer equation (also see Fig 3). Similarly, the Au NPs correspond to the standard PDF 04-0784 (*Fig. 9b*: lattice constants, a = 4.078 Å and α = 90°). The crystallite size of Au nanoparticles was averaged at 10.4 nm; suggesting both Au and

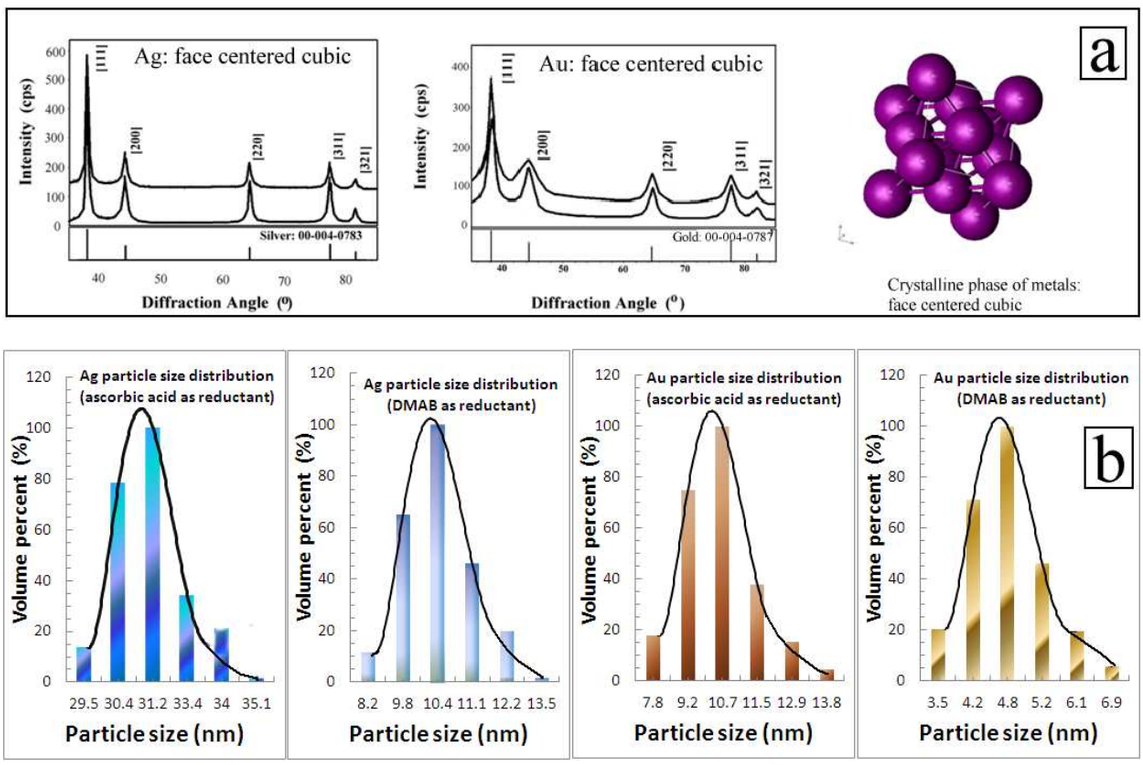

Fig. 9. XRD patterns for nanometals, including XRD patterns for two selected samples, cyrstallite size distribution and cubic centered phase structure, a: XRD pattern of silver and gold nanoparticles and b: particle size distribution of silver and gold nanoparticles.

Ag particle agglomeration was successfully prevented. In both circumstances, the reducing agent, ascorboic acid was selected for demonstration. Other reducing agents provided the same crystalline phase; however, the crystallite size of the engineering particles varies accordingly. It is found that the $NaBH_4$ and DMAB provided essentially the same size, averaged at 12.7 nm for Ag and 4.8 nm for Au nanoparticles, which is also confirmed by TEM measurement. It is important to point out that the lattice occupancy is near ideal (99.0 %), suggesting the Ag and Au nanoparticles possessed highly crystalline structure with less lattice distortion. Both nanoparticles also display high frenquecy of merit (0.2) when using Jade 7.1 database to index with the standard poser diffraction files. The crystalinity index was also determined via taking the ratio of particle size from TEM vs the crystallite size calculated from XRD data. It can be seen that Ag and Au nanoparticles are highly crystalline. Ag showed monoparticles and Au on the other hand polyparticles (see table 2) according to different fabrication methods.

Selected samples	Crystallite size (nm)	Particles size (nm)	Crystallinity	Particle Type
Ag-Ascobic acid	30.2	33.1	≈ 1.1	monocrystalline
Ag- DMAB	12.7	30.4	≈ 2.4	twincrystalline
Ag-DMAB	11.2	34.1	≈ 3.1	polycrystalline
Au-Ascobic acid	10.4	15.6	≈ 1.5	monocrystalline
Au-DMAB	5.8	14.4	≈ 2.2	twincrystalline
Au-DMAB	4.8	15.4	≈ 3.2	polycrystalline

Table 2. Summary of the crystalinity index of Ag and Au nanoparticles (six samples are selected for demonstration)

3.2.3 Fine-structure study of engineered nanomaterials

The morphological and elemental studies through HRTEM technique are shown *(Fig.10a* and *10b*). HRTEM was used as a complementary technique to SEM, which revealed that mono-dispersed and highly crystalline Ag and Au nanoparticles were synthesized. The appearances of both Ag and Au NPs are found to be near-spherical. The particle sizes are varied according to different reducing agents. Generally, the sizes for Ag and Au via reduction of ascorbic acid and citrate are larger than those produced from strong reducing agents, DMAB and $NaBH_4$, with the average particle size from 4.8, to 32 nm in diameter. For both Ag and Ag, ring pattern of the particles indicated that the Ag and Au were well indexed with the standard metallic pattern, which correlated with the XRD analysis.

3.2.4 Elemental composition analyses of engineered nanomaterials

EDS and XPS were used as supplemental techniques to determine the composition of the engineered nanomaterials. EDS spectra of the metal nanoparticles (*Fig. 10a* & *b*, lower right-hand-side panel for elemental analysis) indicated the presence of the Ag and Au elements, noting that metallic Ag displays two major emission lines at K_α: 22.162 keV and L_α: 2.984 keV, respectively. While Au displays two major peaks of L_α at 9.711 keV and M_α 2.123 keV, respectively. The characteristic peaks of Au were obtained, and were correlated to K_α peak

which occurred at 2.10 KeV and the K_β peak which occurred at 2.18 KeV, respectively, which is in agreement with Au characteristic peaks. The Au NP appearance is near-spherical with the average particle size from 15 to 20 nm in diameter. The high resolution image also shows the lattice fringe which was distinguished, which also confirms the formation of Au crystals. The element Cu peak detected is resulting from Cu grid sample holder.

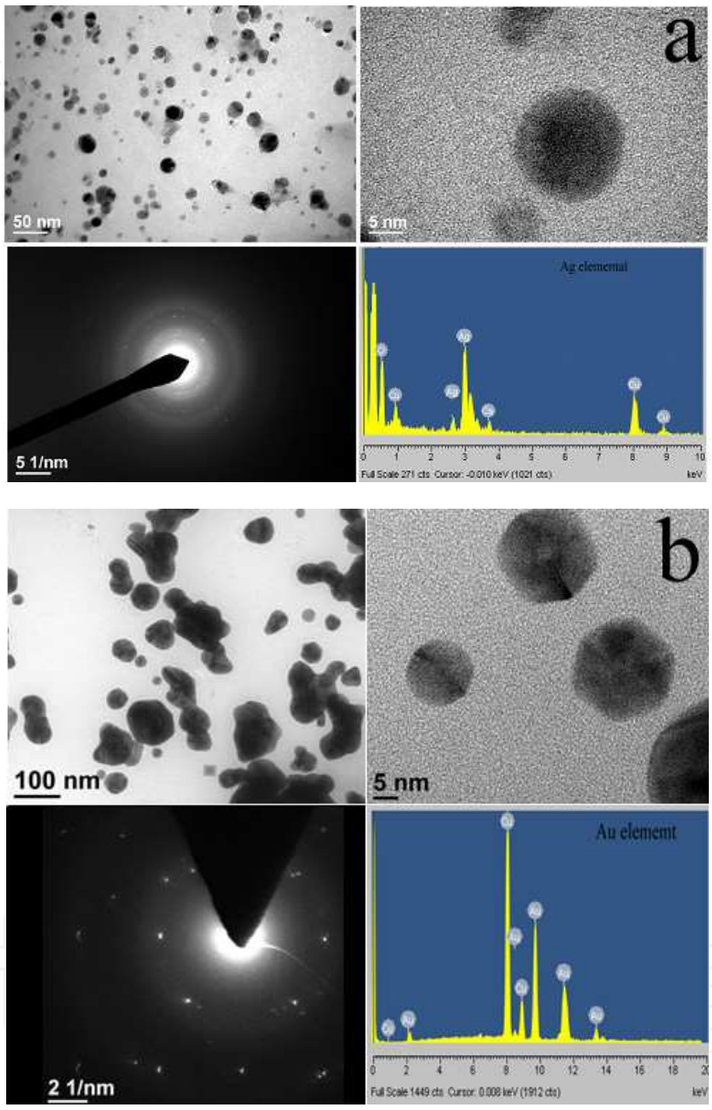

Fig. 10. TEM images and elemental analysis of nanoparticles, a: morphology, ring pattern and composition of nanosilver; b: morphology, ring pattern and composition of nanogold.

The XPS results (*Fig. 11*) show that Ag and Au are characterized by an asymmetric line shape with the peak tailing to the higher BE. The BE may be varied due to its extra columbic interaction between the photoemitted electron and ion core. The binding energies for Ag electron configurations of $3d_{5/2}$ and $3d_{3/2}$ were found to be 366.0 eV and 372.0 eV with the difference of 6.0 eV (Fig. 11a). This measurement was corresponding to the standard Ag 3d binding energies ($3d_{5/2}$ = 368.3 eV, $3d_{3/2}$ = 374.3 eV, Δ = 6.0 eV). Apparently, the 3d

photoemission of Ag is split between two peaks with an intensity ratio at about 6:5. It was also found that Au (Fig. 11b) displayed two principal emissions at $4f_{7/2}$ = 82.2 eV, $4f_{5/2}$ = 85.8 eV, respectively. The spectrum was also well-indexed with the standard metallic Au spectra ($4f_{7/2}$ = 82.2 eV, $4f_{5/2}$ = 85.8 eV, Δ = 3.6 eV).

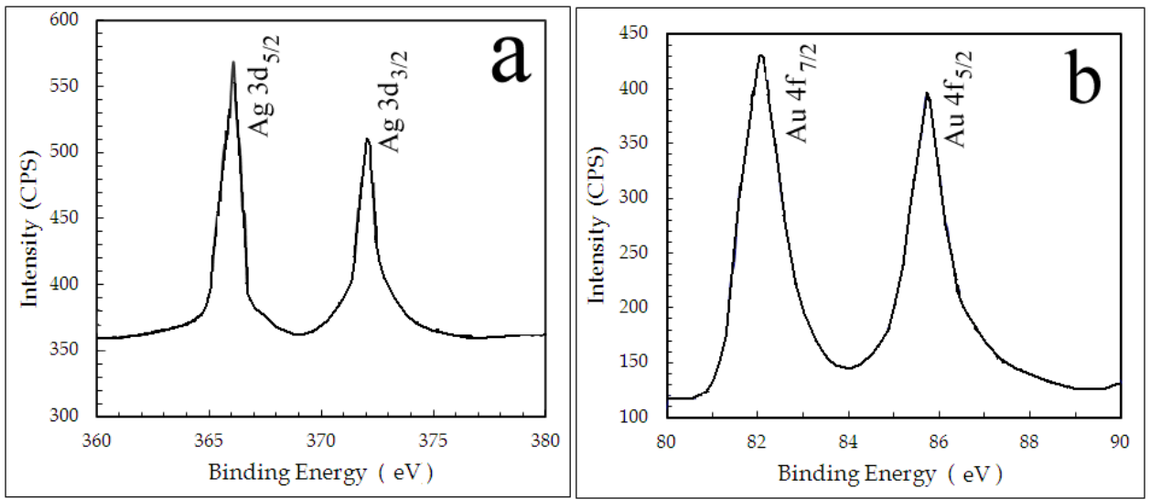

Fig. 11. XPS analyses of NPs, a: determination of nanosilver; b: determination of nanogold.

3.3 *In vitro* cytotoxic activity of nanometals

In addition to nanostructural characterization, the cytotoxicity in normal ovary and ovarian cancer cells using Au and Ag NPs in human red blood cells has been systematically investigated. The *in vitro* cytotoxicity of Ag and Au NPs was assessed in NCI/ADR - RES (OVCAR -8) cells, which are ovarian adenocarcinoma cells, and Chinese hamster ovary (CHO) cells. Samples with 2×10^4 OVCAR-8 and CHO cells were seeded in a 96-well plate. Percentage viability was calculated by comparing absorbance of treated cells with untreated cells (100 % Viability). These results have indicated that at all concentrations (0.1, 0.5, 1, 10 and 100 µM), Au nanoparticles have not shown any toxicity in both normal and ovarian cancer cell lines indicating their biocompatibility. Ag NPs have shown no toxicity at lower concentrations (0.1, 0.5 and 1 µM) in both cell lines. However, at higher concentrations (10 and 100 µM), Ag NPs have shown only 55.9 % and 32.59 % viability in OVCAR-8 cells for 10 and 100 µM doses, respectively. In CHO cells, the Ag NPs have shown 37.88 % and 15.37 % viability for 10 and 100 µM doses, respectively. Based on the data, it may be concluded that the Ag NPs can potentially be used Carriers for cancer therapy. The *in vitro* cytotoxicity data is presented in *Fig. 12a* and *12b.*

3.4 Hemocompatibility of nanometals

Ag and Au NPs were incubated with human red blood cells (RBCs) suspension for 6 hrs in a 96 well plate. The plate was then centrifuged and supernatant was collected and measured for release of hemoglobin by measuring absorbance at 540 nm. RBCs treated with Triton X-100 was used as the reference standard. RBCs are the first point of contact of NPs when administered systemically. In the present study, the Au NPs have shown that the percentage

of hemolysis increased with increase in dose. The Au NPs have shown 9.5 % and 12.5 % hemolysis at 0.1 and 1 μM concentrations, respectively. However, at 10 μM concentrations the % hemolysis was found to be 22.4 %. Similarly, Ag NPs have shown hemolytic profile of 9.47 % and 13.07 % at 0.1 and 1 μM. Interestingly, Ag NPs have also shown higher hemolytic activity 29.15 % at 10 μM. These data suggest that at lower concentrations (0.1, 1 μM), Au and Ag NPs can be used for *in vivo* applications. The *in vitro* hemolysis data are presented in *Fig. 13*.

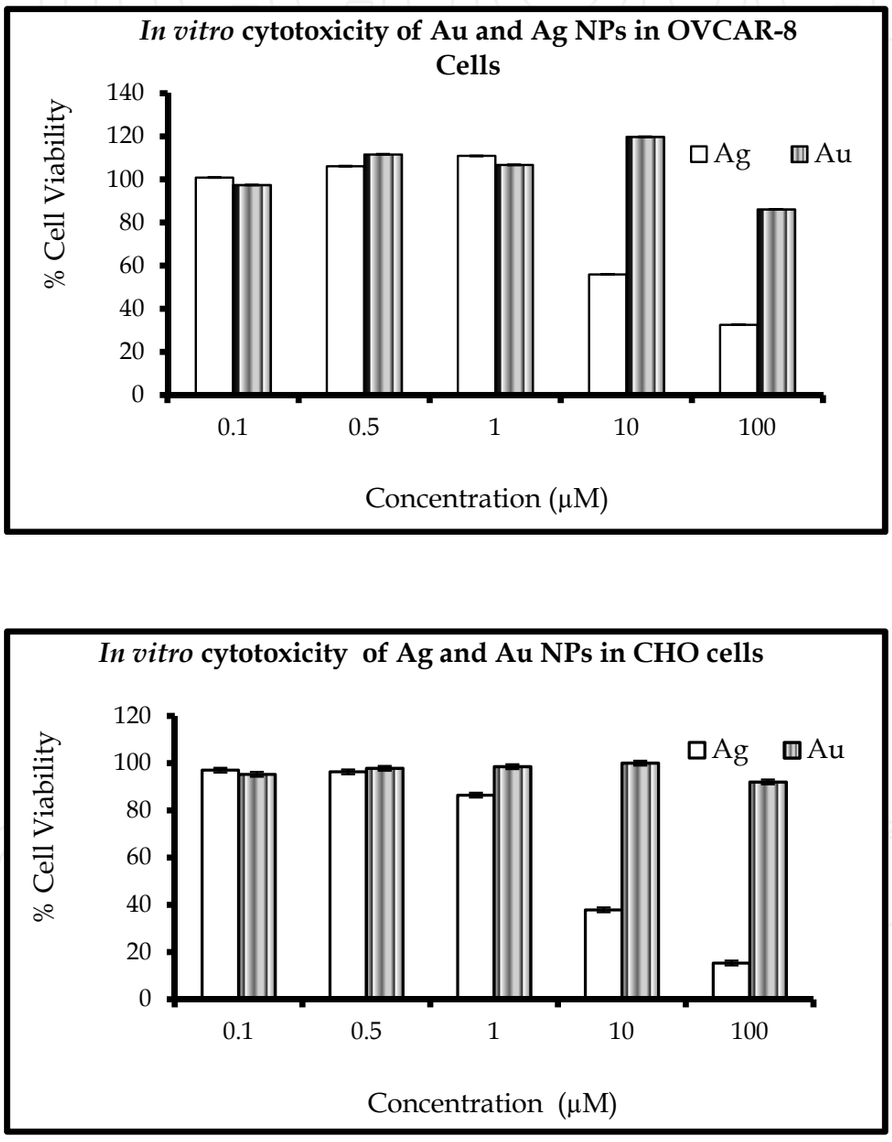

Fig. 12. *In vitro* cytotoxic activity of nanometals, percentage viability was calculated by comparing absorbance of treated cells with untreated cells (100 % Viability), **top panel**: The OVCAR-8 cells were used; **bottom panel**: CHO cells were used.

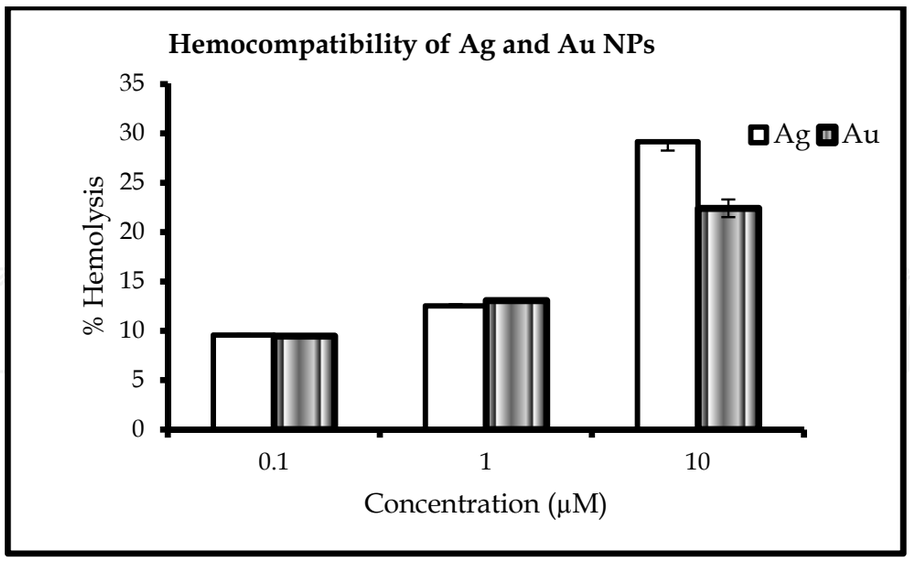

Fig. 13. The hemocompatibility of Ag and Au NPs with human red blood cells, the hollow collum represents the hemocopatibility of Ag, and the filled black colum represents hemocompatibility of Au.

4. Mechanistic studies of nanometals for cancer diagnosis and therapy

A new concept in cancer therapy called "Theragnostics" is emerging recently, which summarizes information based on various biotechnologies involving genomics, transcriptomics, proteomics and metabolomics. [89] The term "Theragnostics" encompasses wide array of topics which includes predictive medicine, personalized medicine, integrated medicine, and pharmacodiagnostics. Major applications of theragnostics in biomedical research include profiling of subgroups of patients based on the likelihood of occurrence of positive outcome to a given treatment so as to entail them to targeted therapies (efficacy), identification of subgroups of patients who are at risk of side effects during a treatment using pharmacogenomics (safety), and monitoring therapeutic response after treatment (efficacy and safety). [90]

The various components of nanotheragnostics each having their own advantage are: signal emitter which emits signal upon excitation by external source, therapeutic moiety can be a drug, or a nucleic acid like small interfering ribonucleic acid (siRNA), nanocarrier is a polymeric carrier capable of carrying high drug payload, and targeting ligand is the entity which can bind to a disease marker with high specificity so as to deliver the entire system to target cell. Non-invasive imaging techniques like magnetic resonance imaging (MRI), X-ray computed tomography (CT), positron emission tomography (PET), single photon emission computed tomography (SPECT), and ultrasound can be used to capture response of signal emitter in real-time. The therapeutic moiety as well as the signal emitter can be encapsulated or covalently attached to the polymeric carrier. Many synthetic and natural polymers were proved to be effective carriers but polymers that are approved for clinical application or currently under clinical trials are poly (ethylene glycol) (PEG), dextran, carboxydextran, β-cyclodextrin, poly (Dextro Levo-lactide-co-glycolide) (PLGA), and poly (L-lysine) (PLL). The

most important component of a theragnositc is its targeting ligand. The targeting ligand includes small molecule ligands like short peptides, aptamers, and large molecule ligands like antibodies.

Metallic nanoparticles because of their unique optical properties and their capability to transit therapeutics to tumor have gained wide importance as theragnostic agents. Au nanoparticles possess unique optical properties such as photothermal and surface-plasmon effects, and these properties can be utilized for various clinical applications in cancer diagnostics. Rod shaped Au NPs (Au nanorods) when irradiated in near-infrared region show a surface Plasmon band. This property can be used for bioimaging, or as heating devices for photothermal therapy. Thus, Au nanorods can be used as potential theragnostic devices for bioimaging, thermal therapy and a drug delivery system. When these Au Nanorods coated with as thermosensitive gel were administered to tumor bearing animals and the tumor was irradiated externally, a significantly larger amount of gold was detected in the irradiated tumor. [91] Ag nanosystems have also shown promise as theragnostic agents because of their optical absorption properties. Ag nanosystems were reported to be potential contrast agents for photoacoustic imaging and image-guided therapy. Ag nanosystems consisting of PEGylated Ag layer deposited on silica Cores were investigated and was shown to be non-toxic *in vitro* at concentrations up to 2 mg/mL. Ag nanosystems also have shown strong concentration-dependent photoacoustic signal when embedded in an *ex vivo* tissue sample. [92] Thus, Ag nanosystems which have capability to carry therapeutic payload and exhibit very strong signal when used for image-guided therapy can be widely used for theragnostic applications.

Theragnostics advanced with advent of nanotechnology. Nanotechnology, by virtue of their unique physicochemical properties like quantum confinement in quantum dots, superparamagnetism in certain oxide nanoparticles and surface-enhanced Raman scattering (SERS) in metallic nanoparticles, resulted in emergence of sensitive and cost effective imaging agents. Similarly, their properties like large surface area to volume ratio, capability to control size, hydrophobicity and surface charge according to intended application made them valuable carriers for therapeutic drugs and genes. [93] Many nanocarriers with anticancer drugs are currently investigated clinically for their targeting capability. Immunoliposomes of doxorubicin are in Phase I clinical trials for targeting human metastatic stomach cancer. [94] Polymeric micelles with Paclitaxel are currently in Phase II clinical trials for targeting stomach cancer. [95] Thus, nanoparticles have the required attributes to house therapeutic payload along with diagnostic imaging agent for real-time monitoring of treatment response.

The Au/Ag-NPs exhibit potential for use for molecular-targeted cancer diagnosis and therapeutics. The Au-NPs were biocompatible with the cell lines utilized in our studies. They exhibit strong absorption at 530 nm in the visible light spectrum, with the absorption maximum wavelength displaying shifts upon interaction with other molecules. They are therefore well suited for the development of diagnostic tools aimed at molecular-targeted detection of cancer cells in samples or *in vivo* through imaging technologies. To achieve molecular targeting, modification of the Au-NPs by conjugation with diverse macromolecules (polypeptides, polysaccharides, and even polynucleotides), is being

explored in our laboratory. The conjugated Au-NPs can be used in the development of contrast agents for optical imaging to identify the cancerous tissues. On the other hand, Ag-NPs showed cytotoxic effects on both the ovarian adenocarcinoma cell line and the non-tumorogenic ovary cell line in the low micromolar range, as well as stronger hemolytic effects with red blood cells. The toxicity properties of Ag-NPs could be utilized for the development of therapeutic agents to eliminate cancer cells. Once again, conjugation with macromolecules could result in novel nanomaterials with enhanced specificity of action. In this case, the macromolecules should either block the toxicity on normal cells, or target the Ag-NPs to the surface of cancer cells specifically. In the latter case, a lower overall concentration of the targeted Ag-NPs could be utilized, which would reach only toxic levels on the surface or within the cancer cells. Oligosaccharide coatings are currently being investigated in our laboratory. The hypothesis is that cancer cells need to grow fast and would have an enhanced requirement for carbohydrates, driving them to accelerated endocytosis of the nanomaterial, reaching therefore toxic levels of Ag-NPs within the cell upon degradation of the oligosaccharide coat. Furthermore, in advanced cancers the leaky blood vessels would release these NPs right near the cancerous cells, providing for another mechanism for concentration of the therapeutic agent at the target sites.

Our laboratory has focused on the coating of NPs with macromolecules that provide a first level of specificity to distinguish cancer cells from healthy cells. Further specificity for diagnosis or treatment of specific cancer types could be achieved by forming hybrid materials that include specific ligands or antibodies that bind to specific cancer cell types. As described earlier, an antibody against the IL13Rα2 receptor has been utilized to direct TiO_2-NPs to certain brain tumors. [78] Our knowledge of molecular markers of specific tumors is increasing steadily, providing tools for the development of a larger collection of high-specificity therapeutic agents that can be utilized in tailored personalized treatment regimens.

5. Conclusion

The green colloidal approach provides stable metallic nanoparticles (Au and Ag). The as-prepared nanometals are determined to be ultrafine, pseudo-spherical and monodispersed. The technical advantages of the colloidal method lie in cost and time effectiveness, simplicity, ability to control homogeneity from molecular level, and high precision of aggregation under use-friendly fabrication variables. The nano-characterization by state-of-the-art instrumentation techniques allow for in-depth understanding of control in morphological, structural and elemental composition via varying the fabrication parameters. Additionally, the Au and Ag nanometals displayed 100 % percentage viability when *in vitro* cytotoxicity was tested. Both metal NPs were also found to be applicable for *in vivo* applications at lower concentrations (0.1, 1 μM).

6. Useful definitions

Phase 0 trials are designed to speed up the development of promising drugs by establishing early on whether they have a similar profile as in the early preclinical studies.

Phase 1 includes trials designed to assess the safety, kinetics, and pharma of a drug.

Phase 2 includes phase I study but on a larger sample size, inculding formulation and dosage.

The Trojan Horse is a stratagem that causes a the nanomaterial to be delivered without detection of the host immune system.

7. Acknowledgements

The authors are grateful to Texas A&M University-Kingsville (TAMUK), the College of Arts and Sciences Research and Development Fund for funding this research activity. The technical support from the National Science Foundation, Major Research Instrumentation program is duly acknowledged to allow the use of JEOL field emission scanning electron microscopy and (TAMUK) Rigaku Ultima III X-ray powder diffraction (TAMU-Corpus Christi). The Academia Mexicana de Ciencias (AMC), Fundación México Estados Unidos para la Ciencia (FUMEC) is also duly acknowledged for their financial support for Dr. Medina-Ramirez to prepare Ag and Au nanoparticles. The Microscope and Imaging Center and the Center of Materials Characterization Facility at TAMU-College Station are also duly acknowledged for technical support and access to the advanced instrumentation, respectively. Last but not least, the authors wish to thank Dr. Sajid Bashir for copy-editing this book chapter.

8. Author contributions

I. Medina-Ramirez conducted the synthesis, and electrokinetic study of nanomaterials. M. Gonzalez-Garcia jointly conceived the conceptual framework with J. Liu and contributed specifically to the application of nanomaterials for cancer diagnosis and treatment. S. Palakurthi completed the toxicicity and hemocompatibility studies. J. Liu prepared Ag and Au nanoparticles based on Medina-Ramirez's discoveries. She completed the spectroscopic and data collection and analysis. She also collected microscopic data with the other investigators (e.g. Dr. Luo at the Materials Characterization Facility and Microscopy Imaging Center) at Texas A&M University-College Station.

9. References

[1] J. Zhang, Z. Liu, B. Han, D. Liu, J. Chen, J. He, T. Jiang, (2004), Chemistry - A European Journal, 10 (14), 3531-3536; Drexler E., Peterson C., Pergamit G. (1991) Unbounding the Future: the Nanotechnology Revolution. William Morrow and Company, New York.

[2] Eric Drexler, Engines of Creation: The Coming Era of Nanotechnology, Bantam Dell Publishing Group Inc (Random House), New York, USA, 1990, pp57-141.

[3] Eric Drexler, Nanotechnology, Molecular Manufacturing, and Productive Nanosystems, John Wiley and Sons Inc, New Jersey, USA, 1991, pp.71-89.

[4] Y. Yao, Y. Ohko, Y. Sekiguchi, A. Fujishima, Y. Kubota, Journal of Biomedical Materials Research Part B: Applied Biomaterials, 2008, 85B, 453.460.

[5] A. Borras, Á. Barranco, J. P. Espinós, J. Cotrino, J. P. Holgado, A. R. González-Elipe, Plasma Processes and Polymers, 2007, 4, 515-527.

[6] F. Zhang, R. Jin, J. Chen, C. Shao, W. Gao, L. Li, N. Guan, Journal of Catalysis, 2005, 232, 424.
[7] A. Kubacka, M. Ferrer, A. Martínez-Arias, M. Fernández-García, Applied Catalysis B: Environmental, 2008, 84, 87-93.
[8] F. Sayılkan, M. Asiltürk, N. Kiraz, E. Burunkaya, E. Arpaç, H. Sayılkan, Journal of Hazardous Materials, 2009, 162, 1309-1316.
[9] A. Mo, J. Liao, W.Xu, S. Xian, Y. Li, S. Bai, Applied Surface Science, 2008, 255, 435.
[10] K. Li, F. S. Zhang, Materials Letters, 2009, 63, 437-441.
[11] F. C. Yang, K. H. Wu, M. J. Liu, W. P. Lin, M. K. Hu, Materials Chemistry and Physics, 2009, 113, 474.
[12] M. Kim, J. W. Byun, D. S. Shin, Y. S Lee, Materials Research Bulletin, 2009, 44, 334-338.
[13] N. Sharifi, N. Taghavinia, Materials Chemistry and Physics, 2009, 113, 63-66.
[14] H. Sakai, T. Kanda, H. Shibata, T. Ohkubo, M. Abe, Journal of American Chemical Society, 2006, 128, 4944-4945.
[15] M. Anpo, M. Takeuchi, Journal of Catalysis, 2003, 216, 505-516.
[16] Y. Ao, J. Xu, D. Fu, C. Yuan, Journal of Physics and Chemistry of Solids, 2008, 69, 2660-2664.
[17] D. Fang, K. Huang, S. Liu, Z. Li, Journal of Alloys and Compounds, 2008, 464, L5-l9.
[18] H. Shibata, T. Ohkubo, H. Kohno, Journal of Photochemistry and Photobiology A: Chemistry, 2006, 181, 357-362.
[19] L. Ge, M. Xu, H. Fang, Journal Sol-Gel Sci Techn, 2006, 40, 65.
[20] D. Wang, F. Zhou, C. Wang, W. Liu, Microporous and Mesoporous Materials, 2008, 116, 658-664.
[21] N. Sobana, K. Selvam, M. Swaminathan, Separation and Purification Technology, 2008, 62, 648.
[22] N. Seirafianpour, S. Badilescu, Y. Djaoued, R. Brüning, S. Balaji, M. Kahrizi, V. Truong, Thin Solid Films, 2008, 516, 6359-6364.
[23] H. Cheng, K. Scott, Journal of Applied Electrochemistry, 2006, 36, 1361-1366.
[24] S. Krishnan, A. C. Kshirsagar, R. S. Singhal, Carbohydrate Polymers, 2005, 62, 309-315.
[25] G. Zhao, S.E. Stevens Jr., BioMetals, 1998, 11, 27-32.
[26] X. G Hou, M. D. Huang, X. L. Wu, A. D. Liu, Chemical Engineering Journal, 2009, 146, 42.48.
[27] J. Sá, C. A. Agüera, S. Gross, J. A. Anderson, Applied Catalysis B: Environmental, 2009, 85, 192-200.
[28] P. Giannouli, R. K. Richardson, E. R. Morris, Carbohydrate Polymers, 2004, 55, 367-377.
[29] M. J. López-Muñoz, J. Aguado, R. V. Grieken, J. Marugán, Applied Catalysis B: Environmental, 2009, 86, 53-62.
[30] S. Bassaid, D. Robert, M. Chaib, Applied Catalysis B: Environmental, 2009, 86, 93-97.
[31] S. K. Ritter, Chemical and Engineering News, 2001, 79(29), 27-34.
[32] L. Picton, I. Bataille, G. Muller, Carbohydrate Polymers, 2000, 2, 23-31.
[33] I. Medina-Ramirez, S. Bashir, Z. Luo, J. Liu, Colloids and Surfaces B: Biointerfaces, 2009, 73, 185-191.
[34] Schrand AM, Rahman MF, Hussain SM, *et al*. Metal-based nanoparticles and their toxicity assessment.Wiley Interdiscip Rev Nanomed Nanobiotechnol 2010;2:544-68.

[35] Li C, Taneda S, Taya K, *et al* .Effects of in utero exposure to nanoparticle-rich diesel exhaust on testicular function in immature male rats.Toxicol Lett 2009;185:1-8.

[36] Wagner AJ, Bleckmann CA, Murdock RC, *et al.* Cellular interaction of different forms of aluminum nanoparticles in rat alveolar macrophages.J Phys Chem B 2007;111:7353-9.

[37] Braydich-Stolle L, Hussain S, Schlager JJ, *et al*. *In vitro* cytotoxicity of nanoparticles in mammalian germline stem cells.Toxicol Sci 2005;88:412-9.

[38] Zhang QL, Li MQ, Ji JW, *et al. In viv*o toxicity of nano-alumina on mice neurobehavioral profiles and the potential mechanisms.Int J Immunopathol Pharmacol 2011;24:23S-29S.

[39] Pan Y, Neuss S, Leifert A, *et al*. Size-dependent cytotoxicity of gold nanoparticles.Small 2007;3:1941-9.

[40] Wang S LW, Tovmachenko O, Rai US, Yu H, Ray PC. Challenge in understanding size and shape dependent toxicity of gold nanomaterials in human skin keratinocytes.Chemical Physics Letters 2008;463:145-49.

[41] Goodman CM, McCusker CD, Yilmaz T, *et al.* Toxicity of gold nanoparticles functionalized with cationic and anionic side chains.Bioconjug Chem 2004;15:897-900.

[42] Shukla R, Bansal V, Chaudhary M, *et al.*. Biocompatibility of gold nanoparticles and their endocytotic fate inside the cellular compartment: a microscopic overview.Langmuir 2005;21:10644-54.

[43] Serda RE, Ferrati S, Godin B, *et al.* Mitotic trafficking of silicon microparticles.Nanoscale 2009;1:250-9.

[44] Kim JS, Yoon TJ, Yu KN, *et al*. Toxicity and tissue distribution of magnetic nanoparticles in mice.Toxicol Sci 2006;89:338-47.

[45] Kim YS, Kim JS, Cho HS, *et al*. Twenty-eight-day oral toxicity, genotoxicity, and gender-related tissue distribution of silver nanoparticles in Sprague-Dawley rats. Inhal Toxicol 2008;20:575-83.

[46] Chen Z, Meng H, Xing G, *et al*. Acute toxicological effects of copper nanoparticles *in vivo*.Toxicol Lett 2006;163:109-20.

[47] Meng H, Chen Z, Xing G, *et al*. Ultrahigh reactivity provokes nanotoxicity: explanation of oral toxicity of nano-copper particles.Toxicol Lett 2007;175:102-10.

[48] Renwick LC, Donaldson K and Clouter A. Impairment of alveolar macrophage phagocytosis by ultrafine particles.Toxicol Appl Pharmacol 2001;172:119-27.

[49] Rothen-Rutishauser B, Grass RN, Blank F, *et al*. Direct combination of nanoparticle fabrication and exposure to lung cell cultures in a closed setup as a method to simulate accidental nanoparticle exposure of humans.Environ Sci Technol 2009;43:2634-40.

[50] Zhang B, Luo Y and Wang Q.Development of silver-zein composites as a promising antimicrobial agent.Biomacromolecules 2010;11:2366-75.

[51] Ren L, Huang XL, Zhang B, *et al.* Cisplatin-loaded Au-Au2S nanoparticles for potential cancer therapy: cytotoxicity, *in vitro* carcinogenicity, and cellular uptake.J Biomed Mater Res A 2008;85:787-96.

[52] E. Traversa, M. L. Vona, P. Nunziante, S. Licoccia, Journal of Sol-Gel Science and Technology, 2001, 22, 115-123.
[53] A. Fujishima, K. Honda, Nature, 1972, 238, 37-38.
[54] V.A. Nadtochenko, A.G. Rincon, S.E. Stanca, J. Kiwi, Journal of Photochemistry and Photobiology A: Chemistry, 2005, 169, 131-137.
[55] T. Saito, T. Iwase, I. Horie, T. Morioka, Journal of Photochemistry and Photobiology B: Biology, 1992. 14, 369-379.
[56] H. Wang, J. Niu, X. Long, Y. He, Ultrasonics Sonochemistry, 2008, 15, 386-392.
[57] G. M. Dougherty, K. A. Rose, J. B. H. Tok, S. S. Pannu, F. Y. S. Chuang, M. Y. Sha, G. Chakarova, S. G. Penn, Electrophoresis, 2008, 29, 1131-1139.
[58] Teoh, W. Yang , Flame spray synthesis of catalyst nanoparticles for photocatalytic mineralization of organics; Ph.D. Thesis, University of New South Wales, 2007, Chapter 1.
[59] J. M Wu, H. C Shih, W.T Wu, Nanotechnology 2005, 17, 105–109.
[60] E.Thimsen, S. Biswas, C. S. Lo, P. Biswas, Journal of Physical Chemistry. C ,2009, 113, 2014–2021.
[61] P.Sangpour, F. Hashemi, A. Z. Moshfegh, Journal of Physical Chemistry. C ,2010, 114, 13955–13961.
[62] S. Shena; L. Guo; X. Chen; F.Ren; C. X. Kronawitter; S.S. Mao, International Journal of Green Nanotechnology: Materials Science & Engineering, 2009, 1, M94 — M104.
[63] X-G Hou, A-D Liu, M-D Huang , B Liao, X-L Wu, Chinese Physics Letters, 2009, 26, 077106-1 to 077106-4.
[64] B.Liang, S. Mianxin, Z. Tianliang, Z.Xiaoyong, D. Qingqing, Journal of Rare Earths, 2009, 27, 461 -468.
[65] S. Chrétien,H.Metiu, 2006, Catalysis Letters, 107, 143-147.
[66] O. Akhavan, Journal of Colloid and Interface Science, 2009, 336, 117-124.
[67] M. S. Chun, H. I. Cho, I. K. Song, Desalination, 2002, 148, 363-367.
[68] Hanahan D, Weinberg RA, 2000. The hallmarks of cancer. Cell 100, 57-70
[69] Vogelstein B, Kinzler KW, 1993. The multistep nature of cancer. Trends Genet 9, 138-141
[70] Vaux DL, Cory S, Adams JM, 1988. Bcl-2 gene promotes haemopoietic cell survival and cooperates with c-myc to immortalize pre-B cells. Nature 335, 440-442
[71] Green DR, Evan GI, 2002. A matter of life and death. Cancer Cell 1, 19-30
[72] Danial NN, Korsmeyer SJ, 2004. Cell death: critical control points. Cell 116, 205-219
[73] Adams JM, Cory S, 2007. The Bcl-2 apoptotic switch in cancer development and therapy. Oncogene 26, 1324-1337
[74] Hermann R, Walther P, Muller M, 1996. Immunogold labeling in scanning electron microscopy. Histochem Cell Biol 106, 31-39
[75] Rand D, Ortiz V, Liu Y, Derdak Z, Wands JR, Taticek M, Rose-Petruck C, 2011. Nanomaterials for X-ray Imaging: Gold Nanoparticle Enhancement of X-ray Scatter Imaging of Hepatocellular Carcinoma. Nano Lett 11, 2678-2683
[76] Bashir S, Chamakura K, Perez-Ballestero R, Luo Z, Liu J, 2011. Mechanism of Silver Nanoparticles as a Disinfectant. International Journal of Green Nanotechnology 3, 118-133

[77] Chamakura K, Perez-Ballestero R, Luo Z, Bashir S, Liu J, 2011. Comparison of bactericidal activities of silver nanoparticles with common chemical disinfectants. Colloids Surf B Biointerfaces 84, 88-96

[78] Rozhkova EA, Ulasov I, Lai B, Dimitrijevic NM, Lesniak MS, Rajh T, 2009. A high-performance nanobio photocatalyst for targeted brain cancer therapy. Nano Lett 9, 3337-3342

[79] Debinski W, Gibo DM, 2000. Molecular expression analysis of restrictive receptor for interleukin 13, a brain tumor-associated cancer/testis antigen. Mol Med 6, 440-449

[80] Mintz A, Gibo DM, Slagle-Webb B, Christensen ND, Debinski W, 2002. IL-13Ralpha2 is a glioma-restricted receptor for interleukin-13. Neoplasia 4, 388-399

[81] Davis ME, 2009. Design and development of IT-101, a cyclodextrin-containing polymer conjugate of camptothecin. Adv Drug Deliv Rev 61, 1189-1192

[82] Lee JH, Huh YM, Jun YW, *et al*.Artificially engineered magnetic nanoparticles for ultra-sensitive molecular imaging.Nat Med 2007;13:95-9.

[83] Thomas TP, Patri AK, Myc A, *et al*. *In vitro* targeting of synthesized antibody-conjugated dendrimer nanoparticles.Biomacromolecules 2004;5:2269-74.

[84] Tallury P, Payton K and Santra S.Silica-based multimodal/multifunctional nanoparticles for bioimaging and biosensing applications.Nanomedicine (Lond) 2008;3:579-92.

[85] Lu CW, Hung Y, Hsiao JK, *et al*. Bifunctional magnetic silica nanoparticles for highly efficient human stem cell labeling.Nano Lett 2007;7:149-54.

[86] Sengupta S, Eavarone D, Capila I, *et al*. Temporal targeting of tumour cells and neovasculature with a nanoscale delivery system.Nature 2005;436:568-72.

[87] Ozdemir V, Williams-Jones B, Glatt SJ, *et al.* Shifting emphasis from pharmacogenomics to theragnostics.Nat Biotechnol 2006;24:942-6.

[88] Pene F, Courtine E, Cariou A, *et al*.Toward theragnostics.Crit Care Med 2009;37:S50-8

[89] Niidome T, Shiotani A, Akiyama Y, *et al*.[Theragnostic approaches using gold nanorods and near infrared light].Yakugaku Zasshi 2010;130:1671-7.

[90] Homan K, Shah J, Gomez S, *et al.* Silver nanosystems for photoacoustic imaging and image-guided therapy.J Biomed Opt 2010;15:021316.

[91] Ho D, Sun X and Sun S. Monodisperse Magnetic Nanoparticles for Theranostic Applications.Acc Chem Res 2011.

[92] Matsumura Y, Gotoh M, Muro K, *et al.* Phase I and pharmacokinetic study of MCC-465, a doxorubicin (DXR) encapsulated in PEG immunoliposome, in patients with metastatic stomach cancer.Ann Oncol 2004;15:517-25.

[93] Matsumura Y. Poly (amino acid) micelle nanocarriers in preclinical and clinical studies.Adv Drug Deliv Rev 2008;60:899-914.

[94] Holzwarth Uwe and Gibson Neil. The Scherrer equation versus the 'Debye-Scherrer equation' Nature Nanotech 2011; 6:534.

[95] Csáki A, Möller R, Straube W, Köhler JM, and Fritzschea W (2001) DNA monolayer on gold substrates characterized by nanoparticle labeling and scanning force microscopy. Nucleic Acids Res. 16:1-5; Garzon´ IL, Artacho E, Beltran´MR, Garc´ia A, Junquera J, Michaelian K, Ordejon´P, Rovira C, Sanchez-Portal´ D, Soler JM (2001) Hybrid DNA-gold nanostructured materials: an ab initio approach. Nanotechnology 12:126–131.

[96] Chen CS (2008) Biotechnology: Remote control of living cells. Nature Nanotechnology 3:13 – 14; Li Z, Jin R, Mirkin CA, Letsinger RL (2002) Multiple thiol-anchor capped DNA–gold nanoparticle conjugates. Nucleic Acids Research 30:1558-1562.

Green Chemistry - Environmentally Benign Approaches
Edited by Dr. Mazaahir Kidwai

ISBN 978-953-51-0334-9
Hard cover, 156 pages
Publisher InTech
Published online 23, March, 2012
Published in print edition March, 2012

Green chemistry is chemistry for the environment. It is really a philosophy and way of thinking that can help chemistry in research and production to develop more eco-friendly solutions. Green chemistry is considered an essential piece of a comprehensive program to protect human health and the environment. In its essence, green chemistry is a science-based non-regulatory and economically driven approach to achieving the goals of environmental protection and sustainable development. Combining the technological progress with environmental safety is one of the key challenges of the millennium. In this context, this book describes the environmentally benign approaches for the industries as well as chemical laboratories. In order to provide an insight into step change technologies, this book was edited by green organic chemists.

InTech Europe
University Campus STeP Ri
Slavka Krautzeka 83/A
51000 Rijeka, Croatia
Phone: +385 (51) 770 447
Fax: +385 (51) 686 166
www.intechopen.com

InTech China
Unit 405, Office Block, Hotel Equatorial Shanghai
No.65, Yan An Road (West), Shanghai, 200040, China
中国上海市延安西路65号上海国际贵都大饭店办公楼405单元
Phone: +86-21-62489820
Fax: +86-21-62489821

IntechOpen